Journal of Catalysis **203,** 382–392 (2001)
doi:10.1006/jcat.2001.3333, available online at http://www.idealibrary.com on IDEAL®

1,3-Butadiene Selective Oxidation over VMoO Catalysts: New Insights into the Reaction Pathway

W. D. Schroeder, C. J. Fontenot, and G. L. Schrader[1]

Department of Chemical Engineering and Ames Laboratory—USDOE, Iowa State University, Ames, Iowa 50011

Received March 5, 2001; revised July 1, 2001; accepted July 1, 2001

The partial oxidation of 1,3-butadiene has been investigated over VMoO catalysts synthesized by sol–gel techniques. Surface areas were 9–14 m^2/g, and compositions were within the solid solution regime, i.e., below 15.0 mol% (MoO_3) in V_2O_5. Laser Raman and XRD data indicated that solid solutions were formed, and pre- and postreaction XPS data indicated that catalyst surfaces were reduced by the 1,3-butadiene-in-air feeds. The reaction pathway for 1,3-butadiene partial oxidation to maleic anhydride was shown to involve intermediates such as 3,4-epoxy-1-butene, crotonaldehyde, furan, and 2-butene-1,4-dial. The addition of water to the reaction stream substantially increased catalyst activity and improved selectivity to crotonaldehyde and furan at specific reaction temperatures.

Key Words: **hydrocarbon selective oxidation; mixed metal oxide catalysts; 1,3-butadiene partial oxidation.**

1. INTRODUCTION

The conversion of 1,3-butadiene to maleic anhydride and other partially oxidized hydrocarbons has been examined using several selective oxidation catalysts. However, there is no generally accepted reaction pathway, particularly regarding the role of specific intermediates and the sequential conversion steps. Most studies have emphasized maleic anhydride production: other compounds such as furan and 3,4-epoxy-1-butene are potentially valuable products also.

Centi and Trifiro suggested a simple consecutive pathway for 1,3-butadiene conversion over VPO catalysts (1):

$$\text{1,3-butadiene} \rightarrow \text{2,5-dihydrofuran} \rightarrow \text{furan} \rightarrow \text{maleic anhydride.}$$

1,4-Cycloaddition of oxygen to 1,3-butadiene produced 2,5-dihydrofuran, followed by allylic H-abstraction to form furan. Maleic anhydride was produced by further oxygen insertion into the 2- and 5-positions. Crotonaldehyde was also detected in these studies but was considered only to be a side product.

Investigations of 1,3-butadiene oxidation over Ag catalysts indicated that 1,4-addition was not the first step in the oxidation of 1,3-butadiene; rather, 1,2-addition was postulated to produce 3,4-epoxy-1-butene (2, 3). Conversion of 1,3-butadiene was inhibited by the epoxide. Reaction of 3,4-epoxy-1-butene over unpromoted Ag catalysts formed furan, crotonaldehyde, acrolein, and CO_2, although only 55% of the converted 3,4-epoxy-1-butene could be accounted for. Experiments using 2,5-dihydrofuran as a feed additive indicated that furan, crotonaldehyde, and CO_2 were formed. Although 3,4-epoxy-1-butene did not produce 2,5-dihydrofuran (and vice versa), it was proposed that the epoxide was the initial 1,3-butadiene oxidation product. Monnier suggested that 3,4-epoxy-1-butene was unable to desorb from the catalyst surface before cyclization to 2,5-dihydrofuran, isomerization to crotonaldehyde, or hydrogenolysis to acrolein. Addition of small amounts of CsCl or CsF produced a highly selective catalyst for 3,4-epoxy-1-butene production from 1,3-butadiene (96% selectivity at 21% conversion). This catalyst proved to also be efficient in the epoxidation of several other compounds, such as styrene, 4-vinylpyridine, and norborene (2, 3). The increase in selectivity was attributed to a lowering of the epoxide desorption energy. Attempts to use these catalysts for the selective oxidation of compounds with allylic hydrogen (propylene, butenes, etc.) were unsuccessful. Apparently, strongly electrophilic oxygen present on the modified Ag surface produced only combustion products.

In other studies over Ag surfaces, the catalytic oxidation of 1,3-butadiene has been considered to be a 1,4-addition where both C=C bonds interact with surface oxygen to form 2,5-dihydrofuran. Studies by Madix *et al.* postulated that for single-crystal Ag (110) surfaces, a stabilized intermediate species was formed which could desorb as 2,5-dihydrofuran. This reaction was compared to a Diels-Alder mechanism for acetylene and 1,3-butadiene conversion to benzene in which interaction of acetylene with the terminal C=C bonds of 1,3-butadiene formed a cyclic structure. In the same fashion, the active oxygen on the catalyst surface was believed to interact with the terminal C=C bonds of 1,3-butadiene to form 2,5-dihydrofuran (4).

[1] To whom correspondence should be addressed.

0021-9517/01 $35.00

Other selective oxidation products generated from 1,3-butadiene have also been detected, suggesting the formation of maleic anhydride by multiple pathways. Akimoto *et al.* observed that over supported molybdena catalysts, maleic anhydride was formed by two temperature-dependent pathways: via 2,5-dihydrofuran with subsequent conversion to furan or via 2,5-dihydrofuran only (5). More recent work by several research groups has suggested that these multiple pathways were a result of ring opening of cyclic compounds and subsequent reaction of "open-chain" compounds. Recyclization of the partial oxidation intermediates could then produce maleic anhydride. Crew and Madix performed ^{18}O labeling experiments over a Ag (110) catalyst using furan as the reactant (6). In their experiments furan underwent ring opening before maleic anhydride formation. Xue and Schrader conducted transient *in situ* FTIR studies over $(VO)_2P_2O_7$ to demonstrate similar pathways for the oxidation of methyl vinyl ketone, crotonaldehyde, 1,3-butadiene, 2,5-dihydrofuran, furan, and 2(5*H*)-furanone (7). Cyclic compounds [2,5-dihydrofuran, furan, and 2(5*H*)-furanone] were converted to maleic anhydride, but only after initial ring cleavage produced open-chain carbonyl compounds such as crotonaldehyde or 2-butene-1,4-dial. In addition, crotonaldehyde and methyl vinyl ketone formed maleic anhydride with no evidence of prior cyclization. Hönicke proposed multiple pathways to maleic anhydride over V_2O_5 catalysts (Fig. 1). Furan was produced directly from crotonaldehyde, 2,5-dihydrofuran, and 2,3-dihydrofuran, and the immediate precursors for maleic anhydride were 2-butene-1,4-dial, 2(5*H*)-furanone, and furan (8, 9).

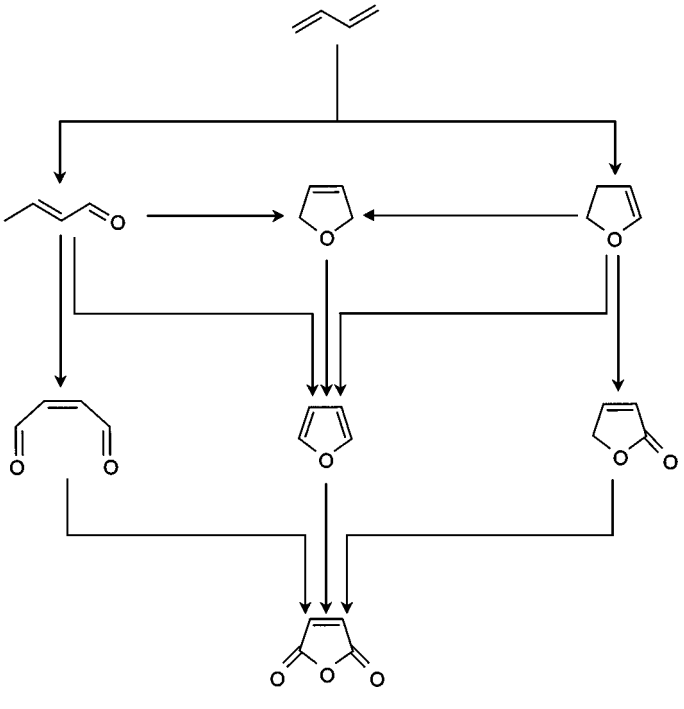

FIG. 1. Reaction pathway of 1,3-butadiene to maleic anhydride over V_2O_5 proposed by Hönicke *et al.*

The objective of our current research has been to further elucidate the reaction pathway for 1,3-butadiene-selective oxidation to valuable products such as maleic anhydride and furan. VMoO catalysts have been prepared that can produce these key products as well as other important reaction intermediates. Several characterization techniques have been utilized to examine the catalytic solid solution materials. Addition of water has also been shown to affect the selectivity of the VMoO catalysts for intermediates such as furan and crotonaldehyde.

2. METHODS

2.1. Preparation of VMoO Catalysts by Sol–Gel Synthesis

Samples having compositions of 3.5 (Catalyst A) and 14.0 mol% MoO_3 in V_2O_5 (Catalyst B) were prepared using a hydrogen peroxide-based, sol–gel preparation method (10–13). $(NH_4)_2MoO_4$ (Fisher Scientific) was added to deionized water and gently heated to ensure complete dissolution. In a separate flask, V_2O_5 (99.9%, Alfa-Aesar) was added to deionized water and stirred. After approximately 5 min, a 30% aqueous solution of H_2O_2 (Fischer Scientific) was added to the V_2O_5–H_2O slurry. Within minutes the solution turned from orange to clear red, and the molybdate solution was added. The solution turned dark red and then light orange or yellow. After a few minutes, a colloidal gel formed and settled on the bottom of the flask under a layer of solvent. The gel of Catalyst A was brown while the gel of Catalyst B was dark green. Once the gel had formed, the remaining water was poured off the samples, and the gels were covered with *n*-pentane. After 3 days, the catalysts were allowed to dry at ambient conditions and then calcined for 4 h at 350°C. The calcined powder appeared green-black and shiny.

2.2. Catalyst Characterization

2.2.1. Surface Area Measurements

Surface areas were measured using the BET method. A Micromeretics ASAP 2000 surface analysis system was used with N_2 as the adsorbate.

2.2.2. Laser Raman Spectroscopy

Laser Raman spectroscopy (LRS) was performed in a backscattering mode using a fiber-optic probe head coupled to a Kaiser Holospec f/1.8 spectrometer. A Coherent 532-50 diode-pumped solid-state laser was the excitation source (532 nm, 50 mW at the source), and a Princeton Instruments CCD (1100 × 330) detector system was used with Winspec acquisition and processing software.

2.2.3. X-Ray Diffraction (XRD)

XRD was performed using a Scintag 2000 diffractometer utilizing CuK_α radiation. Standard powder diffraction was performed for the solid-state synthesis products. Diffraction patterns were recorded using θ–2θ scans between 10 and 70° with 0.050° step size in 2θ and 2.0 s count per step time.

2.2.4. X-Ray Photoelectron Spectroscopy

X-ray photoelectron spectroscopy (XPS) was performed using a Physical Electronics Multitechnique system with monochromatic Al at 29.35 eV. The base pressure for the analyzer system was less than 3×10^{-10} Torr. Postreaction catalyst samples were sealed in their reactor tubes under He and transferred to a glove box under an inert atmosphere. Samples were then loaded into the analysis chamber without exposure to the atmosphere.

2.3. Reactor Studies

Reactions were performed using the system shown in Fig. 2. The gas feed composition ranged from 0.5 to 1.4% 1,3-butadiene (Matheson, C.P. grade) in 77–92% air (Air Products, zero grade) and 8–22% He (Air Products, zero grade). Hydrocarbon product feeds were introduced to the reactor system using a He-swept liquid saturator in which both temperature and He flow could be adjusted. For low temperatures (less than −20°C), a liquid N_2-cooled ethanol bath was required. For saturator temperatures above −20°C, a commercial ethylene glycol temperature bath was used (Brinkmann Instruments). These hydrocarbon feeds were maintained below 0.15% of the total feed (51% air and balance He). A 2.5% water additive level was introduced into the feed by directing the air stream through a saturator at 22°C. Helium was added to maintain a constant flow rate.

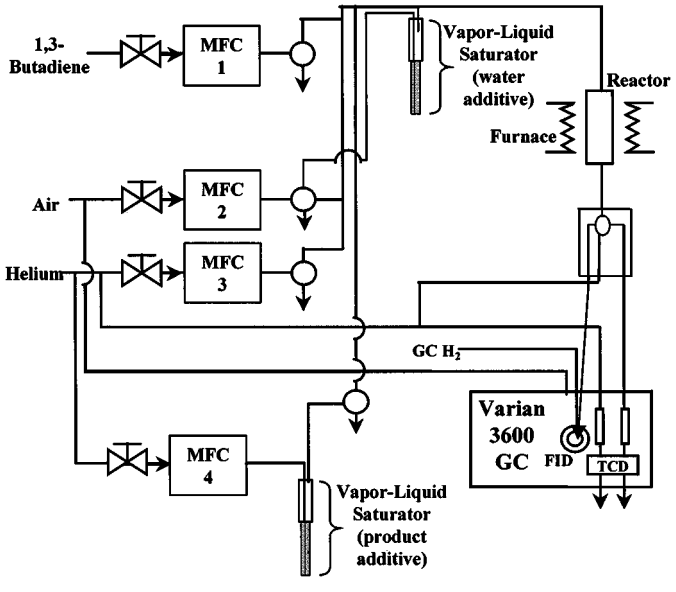

FIG. 2. Reactor system for selective oxidation of 1,3-butadiene and other hydrocarbons over V–Mo–O catalysts.

Catalysts were pressed and sieved (ca. 0.15 g, 40/100 mesh) before being loaded into the continuous-flow reactor (6 mm i.d., quartz). Differential conversion conditions were maintained for all 1,3-butadiene studies. Small amounts of quartz wool were packed above and below the catalyst bed. Temperatures were maintained between 110 and 300°C using a programmable temperature controller (Omega Engineering). Feed and effluent lines were heated to 150°C to prevent product condensation. Total flow rates were regulated from 70 to 200 sccm using mass flow controllers.

The Varian 3600 gas chromatograph used a Carbosphere 80/100 packed column for the thermal conductivity (TCD) and a CP-Select 624 CB mega-bore capillary column (Varian, Inc.) for the flame ionization detector (FID). Sample loop size was 1.0 mL. For these studies, the percentage conversion of 1,3-butadiene was defined as

$$\frac{\text{moles 1,3-butadiene reacted}}{\text{moles 1,3-butadiene fed}} \times 100.$$

Percentage selectivity to a specific product was defined as

$$\frac{\text{moles product}}{\text{moles 1,3-butadiene reacted}} \times \frac{1}{\gamma} \times 100,$$

where γ was the stoichiometric carbon atom ratio of 1,3-butadiene (4) to a product.

3. RESULTS

3.1. Characterization of VMoO Catalysts Prepared by Sol–Gel Synthesis

3.1.1. Surface Area

The prereaction surface area of Catalyst A was determined to be 9.1 m^2/g. Postreaction surface area was 8.3 m^2/g. Prereaction surface area for Catalyst B was determined to be 13.4 m^2/g. Postreaction surface area was 12.0 m^2/g. These higher surface areas were achieved by solvent exchanging *n*-pentane for the water that was trapped in the gel pores during synthesis. Replacing a high surface tension solvent (water) with a low surface tension solvent (*n*-pentane) probably decreased pore collapse, which may have occurred during the drying process.

3.1.2. Laser Raman Spectroscopy

Raman spectra for pre and postreaction catalysts have been presented in Fig. 3. For Catalyst A, low wavenumber bands at 406, 300, 283, and 201 cm^{-1} were characteristic of vanadium–oxygen bending vibrations (14). The 990, 689, and 523 cm^{-1} peaks were likely related to stretching

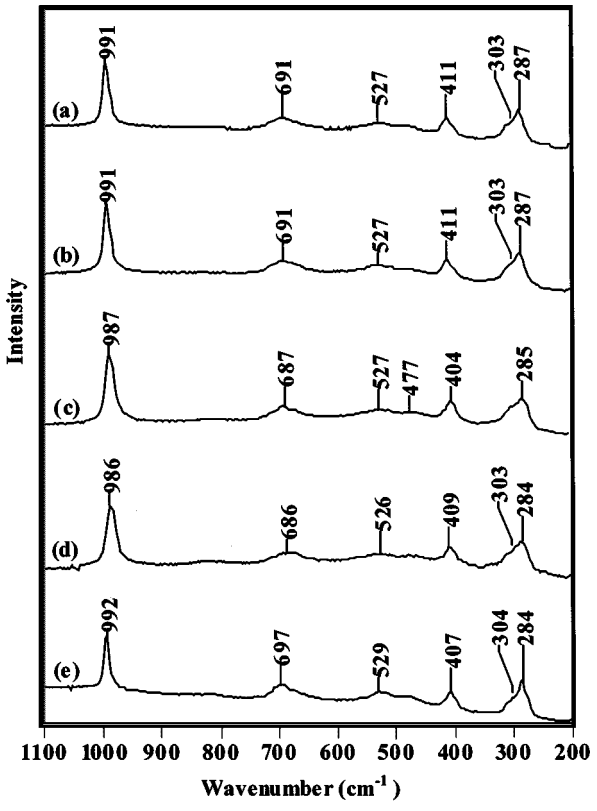

FIG. 3. LRS of VMoO catalysts. (a) Catalyst A prereaction, (b) catalysts A postreaction, (c) catalyst B prereaction, (d) catalyst B postreaction, (e) V_2O_5 reference. These spectra were all collected in 3-min acquisition times under 50 mW laser power at 532 nm.

vibrations (995, 701, and 527 cm^{-1} for V_2O_5) and were assigned to terminal V=O, edge-sharing V–O, and corner sharing V–O–V stretching frequencies, respectively. The downward shift of these bands has been explained in terms of solid solution formation (23). Postreaction Raman characterization indicated virtually no shifts in peak positions.

For Catalyst B, the Raman spectrum was similar to that for V_2O_5. However, a somewhat larger shift of the 995 cm^{-1} band to 987 cm^{-1} was observed. Raman band positions following reaction were virtually unchanged.

3.1.3. *X-Ray Diffraction*

X-ray powder patterns have been presented in Fig. 4 (also for crystalline V_2O_5). XRD results for Catalyst A prior to reaction were similar to V_2O_5 except for small shifts in *d*-spacing. The *d*-spacing measurements for selected representative Miller indices of the pre and postreaction catalysts have been reported in Table 1. Incorporation of Mo in the vanadia catalysts resulted in expansion of the *d*-spacing in the (100) and (010) directions and contraction in the (001) direction. Postreaction XRD characterization indicated little change in the long-range order of Catalyst A or B.

TABLE 1

XRD *d*-Spacing Measurements for V_2O_5, Catalyst A and Catalyst B

Lattice plane	V_2O_5 reference	Catalyst A		Catalyst B	
		Prereaction	Postreaction	Prereaction	Postreaction
100	11.54	11.55	11.56	11.60	11.61
010	3.57	3.57	3.57	3.59	3.59
001	4.38	4.36	4.37	4.33	4.32

Note. Data in Å.

3.1.4. *X-Ray Photoelectron Spectroscopy*

Results from X-ray photoelectron spectroscopy (XPS) of Catalysts A and B before and after reaction have been presented in Table 2, and the spectra for the vanadium region of the spectrum have been provided in Figs. 5 and 6. The strong oxygen (O 1*s*) signal on the catalyst surfaces was used to calibrate the XPS spectra (15). For the prereaction materials, V binding energies decreased with addition of Mo. Following reaction, there was an additional decrease in V binding energies. The data for Figs. 5 and 6 were fitted to the standard doublets for V^{5+} (V $2p_{3/2}$ at 517.4 eV and V $2p_{1/2}$ at 525.0 eV) and V^{4+} (V $2p_{3/2}$ at 515.4 eV and V $2p_{1/2}$ at 523.0 eV) (16, 17).

For Catalyst A, V^{5+} was predominant, but a relatively small amount of V^{4+} (about 6%) was also detected. For the postreaction spectra, the V bands shifted due to an increase in V^{4+}. After reaction, approximately 20% of the intensity of the V signal could be attributed to V^{4+} (Table 2), which revealed significant surface reduction. For Catalyst B, V^{5+} also appeared to dominate the oxidation state of the prereaction catalyst, although the proportion of V^{4+} (about 9%) was larger. Postreaction XPS characterization revealed further reduction (about 12%).

Molybdenum appeared to exist only in the Mo^{6+} oxidation state in Catalysts A and B. Only a single doublet for Mo was observed. Pre and postreaction Mo binding energies

TABLE 2

XPS Data for Peak Positions for Vanadium and Molybdenum and Intensities of Fitted V^{4+} and V^{5+} Peaks for Catalysts A and B

	Catalyst A		Catalyst B	
	Prereaction (eV)	Postreaction (eV)	Prereaction (eV)	Postreaction (eV)
V $2p_{3/2}$	517.2	517.0	517.1	517.0
V $2p_{1/2}$	524.9	524.3	524.6	524.6
Mo $3d_{5/2}$	235.8	235.7	235.8	235.7
Mo $3d_{3/2}$	232.6	232.5	232.6	232.6
V^{4+}/V_{Total}	6.2%	20%	9.3%	12%

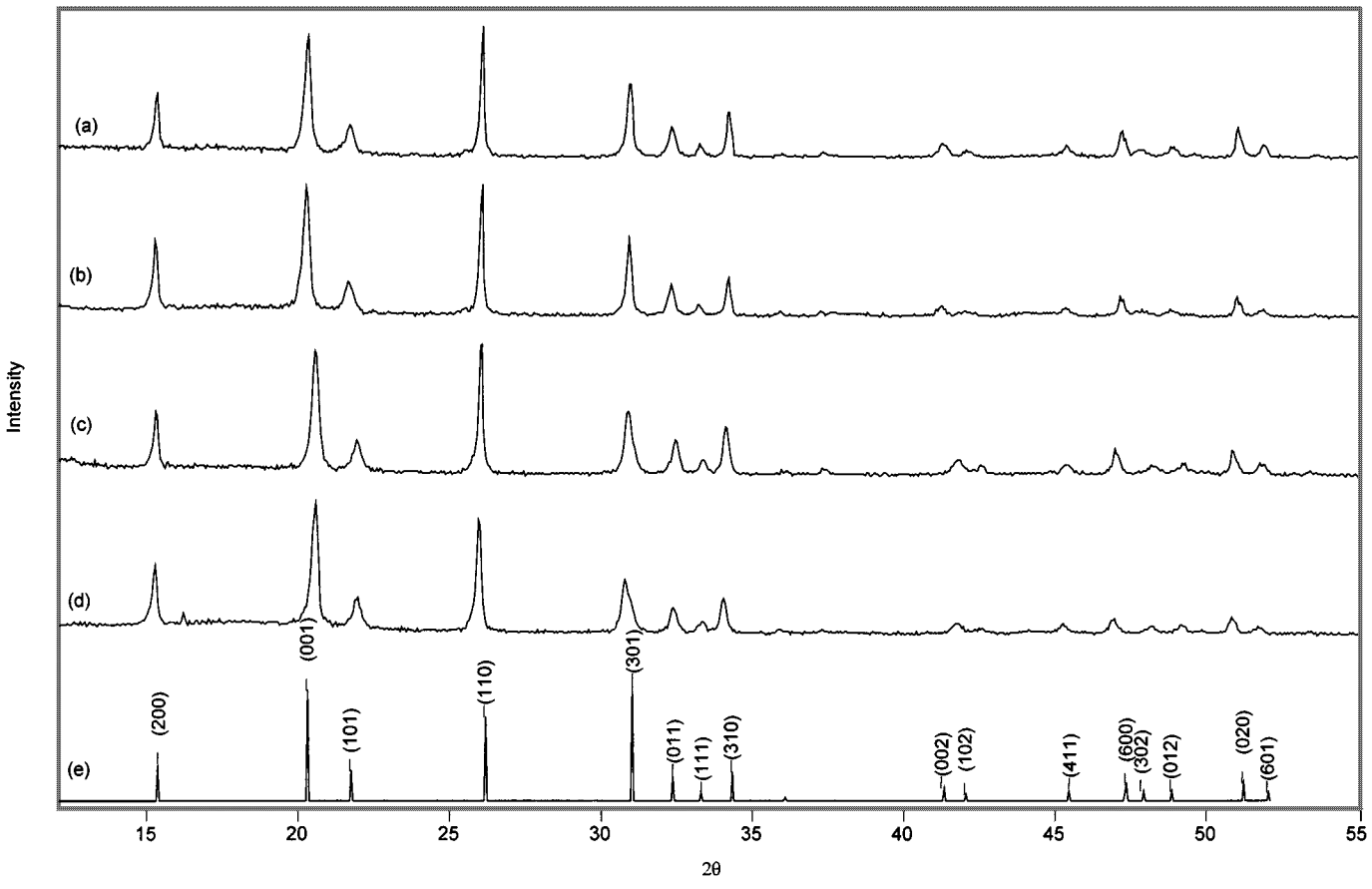

FIG. 4. XRD of VMoO catalysts. (a) Catalyst A prereaction, (b) catalyst A postreaction, (c) catalyst B prereaction, (d) catalyst B postreaction, (e) V_2O_5 reference.

were similar to the doublet for Mo^{6+} based on MoO_3 (Mo $3d_{5/2}$ at 235.8 eV and Mo $3d_{3/2}$ at 232.7 eV) (18).

3.2. Reactor Studies

3.2.1. Effect of Catalyst Composition

Product selectivities for Catalysts A, B, and V_2O_5 at 275°C have been summarized in Fig. 7 for 5% conversion of 1,3-butadiene. Reaction products included 3,4-epoxy-1-butene, furan, 2-butenal (crotonaldehyde), acrolein, 2-butene-1,4-dial, maleic anhydride, CO_x, phthalic anhydride, and 2(5*H*)-furanone. Phthalic anhydride and 2(5*H*)-furanone were detected in trace quantities (selectivity less than 1%).

For higher Mo concentrations, selectivities to furan and CO_x decreased while selectivity to maleic anhydride tended to increase. Selectivies to 3,4-epoxy-1-butene, 2-butene-1,4-dial, and crotonaldehyde remained relatively unchanged, and the selectivity to 2-butene-1,4-dial decreased slightly.

3.2.2. Effect of Temperature

Temperature studies between 230 and 300°C were performed for Catalyst B using a 200 sccm feed of 0.5% 1,3-butadiene in air. Conversion of 1,3-butadiene remained less than 5% for these studies. Product selectivity as a function of temperature has been presented in Fig. 8. As temperature increased, selectivities to CO_x and maleic anhydride increased, while selectivities to 3,4-epoxy-1-butene, crotonaldehyde, and 2-butene-1,4-dial decreased. Selectivity to furan appeared to reach a maximum around 275–285°C.

3.2.3. Reaction of Other Partially Oxidized Hydrocarbons

The conversion of 3,4-epoxy-1-butene, crotonaldehyde, furan, and 2,5-dihydrofuran were examined from 180 to 280°C. Catalyst B was used for these studies. Concentrations of these feeds were approximately 0.15% in air with added He to achieve a total flow rate of 105 sccm.

3,4-Epoxy-1-butene. Conversion of 3,4-epoxy-1-butene and product selectivities as a function of temperature have been presented in Fig. 9. The reaction products for 3,4-epoxy-1-butene oxidation were crotonaldehyde, furan, 2-butene-1,4-dial, maleic anhydride, and CO_x. At lower temperatures, some 2,5-dihydrofuran was detected (maximum selectivity of about 15% at 180°C, although higher levels were possible at lower temperatures). Conversion of

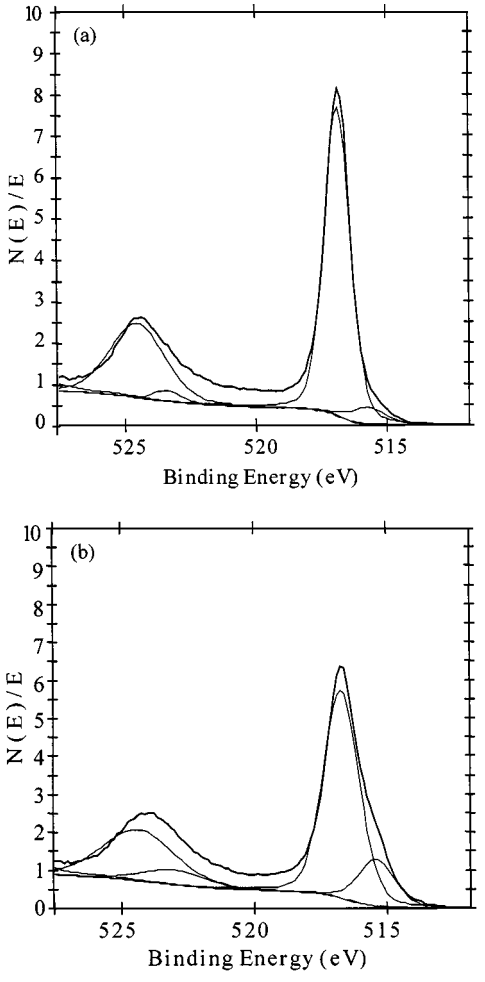

FIG. 5. XPS of VMoO catalysts (V region) for (a) catalyst A prereaction and (b) catalyst A postreaction.

3,4-epoxy-1-butene was near 20% at 180°C and increased to near 100% around 260°C. Selectivities to crotonaldehyde and 2-butene-1,4-dial appeared to reach maxima at 200°C; furan reached a maximum near 240°C; and maleic anhydride appeared to approach a maximum at 280°C.

Crotonaldehyde. Conversion of crotonaldehyde and product selectivities have been presented as a function of temperature in Fig. 10. Crotonaldehyde produced acrolein, furan, 2-butene-1,4-dial, maleic anhydride, and CO_x. Neither 3,4-epoxy-1-butene nor 2,5-dihydrofuran were detected in the reactor effluent. At higher temperatures, conversion increased and more CO_x was produced while selectivities to furan and 2-butene-1,4-dial achieved maxima around 240°C. The selectivity to maleic anhydride apparently went through a minimum around 225°C.

Furan. Only maleic anhydride and CO_x were produced from furan, but conversion was insignificant until 220°C (Fig. 11); at temperatures above 280°C, conversion increased significantly. Selectivity to maleic anhydride decreased with increasing temperature (from almost 95% at 220°C to 60% at 280°C). CO_x selectivity increased with temperature.

2,5-Dihydrofuran. The reaction products for 2,5-dihydrofuran oxidation were furan, maleic anhydride, and CO_x (Fig. 12). 3,4-Epoxy-1-butene, crotonaldehyde, acrolein, or 2-butene-1,4-dial were not detected in the reactor effluent stream. As temperature was increased, conversion to 2,5-dihydrofuran increased from 35 to 100%. Selectivity to CO_x also increased with temperature, while selectivity to furan was nearly 95% at 180°C. Maleic anhydride selectivity appeared to reach a maximum of about 65% around 265°C.

3.2.4. Effects of Water Addition

Addition of 2.5% water to the 1.4% 1,3-butadiene feed resulted in a 40% increase in conversion. Selectivities to furan, crotonaldehyde, and 3,4-epoxy-1-butene also

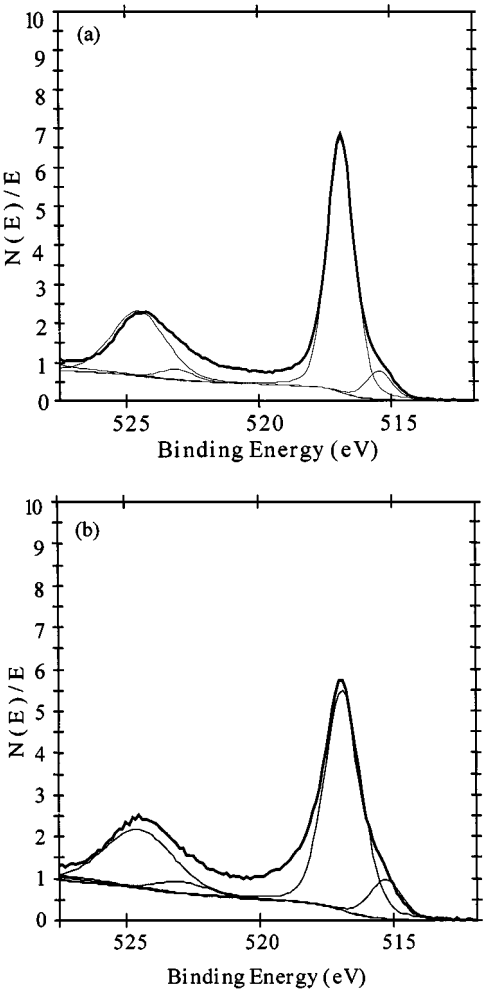

FIG. 6. XPS of VMoO catalysts (V region) for (a) catalyst B prereaction and (b) catalyst B postreaction.

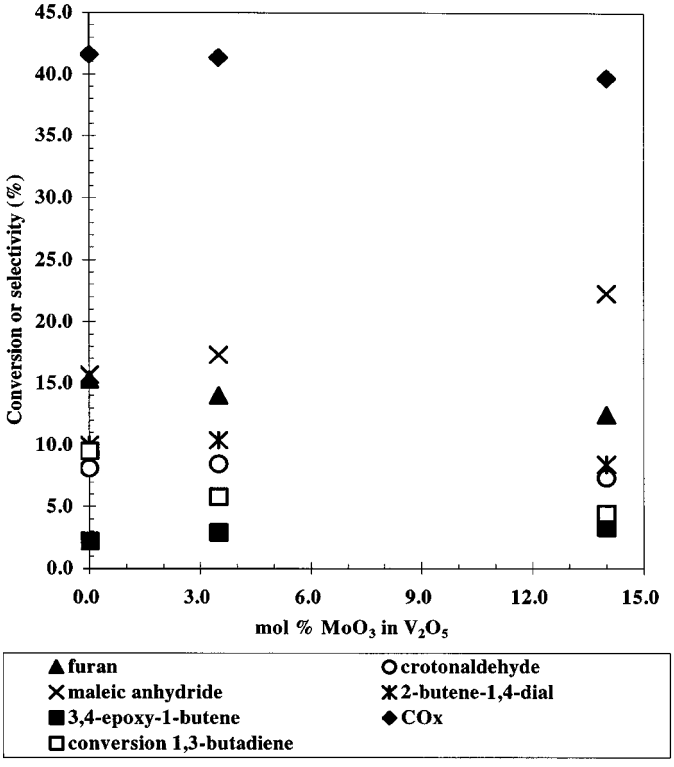

FIG. 7. Effect of Mo concentration for selective oxidation of 1,3-butadiene at 275°C. Total gas flow rate was 70 sccm (1.4% 1,3-butadiene in air and He) and conversion was near 5.0%.

increased while those for CO_x and maleic anhydride decreased (Fig. 13). Following the water addition experiments, the catalysts were reexamined without added water. Catalyst performances were similar to the prior studies not involving water addition.

4. DISCUSSION

Based on these studies, a reaction pathway for the selective oxidation of 1,3-butadiene to maleic anhydride over VMoO catalysts has been proposed (Fig. 14). According to this pathway, 1,2-addition of electrophilic oxygen to 1,3-butadiene first produced 3,4-epoxy-1-butene. This initial step was confirmed by the feed additive studies in which conversion of 3,4-epoxy-1-butene also produced compounds from 1,3-butadiene oxidation. The role of 3,4-epoxy-1-butene as the initial product of 1,3-butadiene oxidation was further indicated by the temperature variation experiments: as 1,3-butadiene conversion decreased at lower temperatures, selectivity to 3,4-epoxy-1-butene increased.

In the next step of the reaction pathway, 3,4-epoxy-1-butene underwent isomerization to crotonaldehyde, the dominant product at low conversions. The transformation of 3,4-epoxy-1-butene to crotonaldehyde was considered to

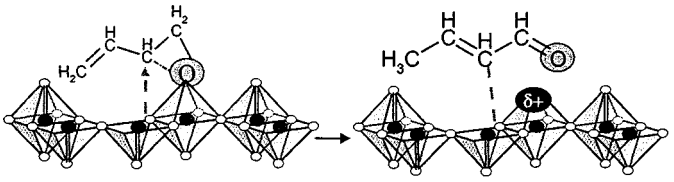

SCHEME 1

be an acid-catalyzed ring-opening of the bond between carbon 3 and oxygen. The epoxide oxygen coordinated to the acidic surface site induced the nucleophilic coordination (see Scheme 1).

2,5-Dihydrofuran was also a reaction product of 3,4-epoxy-1-butene conversion, but only trace quantities were detected. Feed additive studies using 3,4-epoxy-1-butene supported this understanding. At similar temperatures, 2,5-dihydrofuran was significantly more reactive than 3,4-epoxy-1-butene, crotonaldehyde, or furan. Although other researchers have found that 2,5-dihydrofuran oxidation over silver-based epoxidation catalysts produced crotonaldehyde, only furan and maleic anhydride (and CO_x) were detected in our studies (2, 3). The conversion of 3,4-epoxy-1-butene to 2,5-dihydrofuran has been proposed to be only a minor alternate route for the mechanism shown in Fig. 14.

Crotonaldehyde produced furan, maleic anhydride, and 2-butene-1,4-dial, and a dual pathway to both furan and

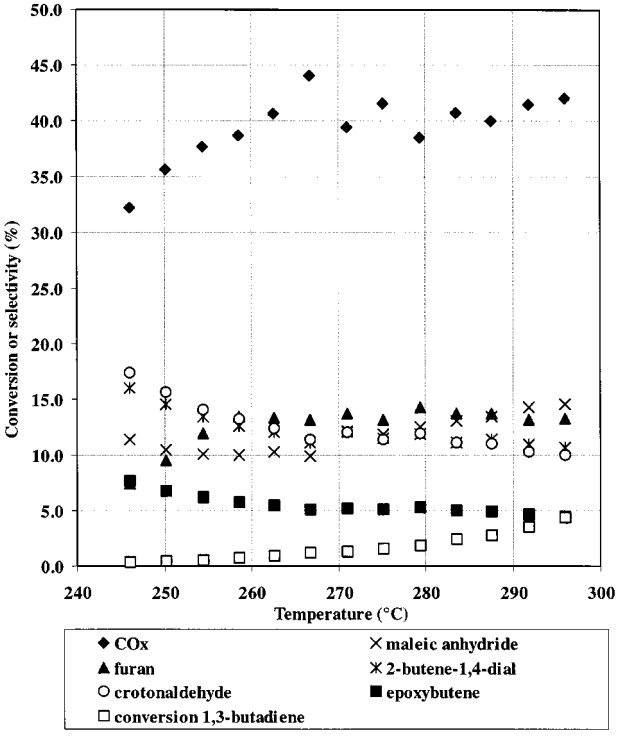

FIG. 8. Effect of temperature between 240 and 300°C for 1,3-butadiene-selective oxidation over Catalyst B. Total gas flow rate was 200 sccm (0.5% 1,3-butadiene in air and He).

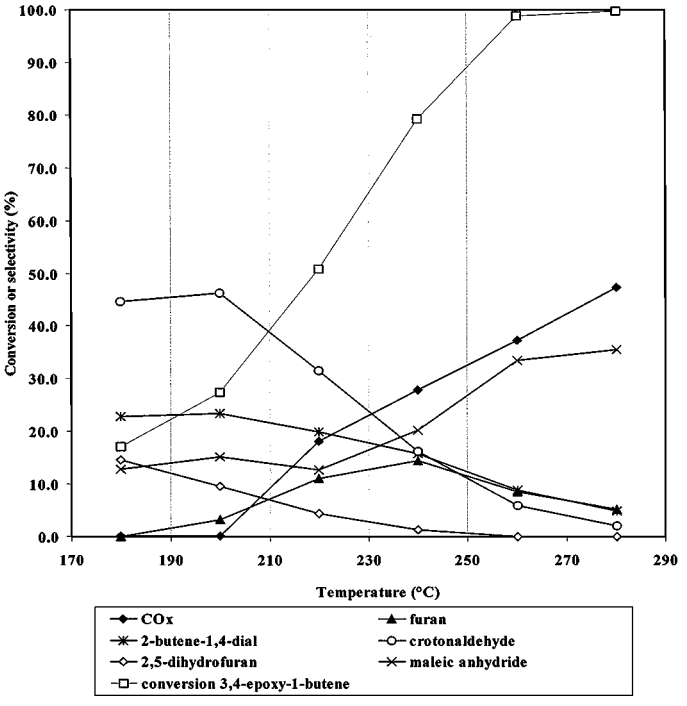

FIG. 9. Effect of temperature between 180 and 280°C for 3,4-epoxy-1-butene-selective oxidation over Catalyst B. Total gas flow rate was 105 sccm (0.15% 3,4-epoxybutene in air and He).

2-butene-1,4-dial has been proposed in Fig. 14. Allylic hydrogen abstraction and subsequent ring closure produced furan, and allylic hydrogen abstraction combined with nucleophilic oxygen insertion at the allylic center formed 2-butene-1,4-dial. Temperature studies revealed similarities in selectivity trends for crotonaldehyde and 2-butene-1,4-dial, likely indicating a common precursor.

Reaction of furan produced maleic anhydride and small amounts of 2(5*H*)-furanone. Xue *et al.* observed ring opening for furan and 2(5*H*)-furanone for VPO catalysts, but the VMoO solid solution materials apparently did not catalyze these reactions (7). These transformations, however, could have occurred on the surface with no desorption and detection of the intermediate species. This possibility, however, was discounted since products of ring opening such as crotonaldehyde should have been evolved from the VMoO surface. 2(5*H*)-Furanone was also a possible intermediate in the reaction of furan to maleic anhydride. Our studies indicated that 2(5*H*)-furanone either was quickly converted to the more stable maleic anhydride species (in a manner similar to 2,5-dihydrofuran) or was strongly adsorbed on the surface. The conversion of 2-butene-1,4-dial to maleic anhydride has been proposed over VPO, Ag, and V_2O_5-based catalysts (6, 8). The instability of 2-butene-1,4-dial and lack of commercial availability made confirmation of this pathway impossible for our studies.

For the VMoO catalysts, an increase in molybdenum content increased the selectivity to maleic anhydride but decreased conversion of 1,3-butadiene. The catalyst having a composition expressed as 14.0 mol% MoO_3 in V_2O_5 (near saturation of Mo in V_2O_5) had the highest selectivity for maleic anhydride. Catalysts with lower Mo content produced relatively more furan and crotonaldehyde. Catalyst B apparently had a higher tendency to promote nucleophilic addition reactions, resulting in oxidation to maleic anhydride while the active sites in Catalyst A and pure V_2O_5 possessed more electrophilic nature associated with the initial epoxidation step.

The XRD and XPS characterization performed on Catalysts A and B supported formation of solid solutions of Mo in V_2O_5. The lattice expansion in the (100) and (010) planes and contraction in the (001) plane indicated that Mo directly replaced V in the VMoO catalysts. The magnitude of lattice shift in this work was 0.01–0.05 Å, significantly less than that observed for the single crystal studies done by Kihlborg, in which lattice spacing shifted on the order of 0.1 Å for the saturated VMoO solid solution. It seems likely that the solid solution structure of Catalyst B was more similar to V_2O_5 than the *R*-Nb_2O_5 proposed by Kihlborg, possibly a result of our synthesis technique (19, 20). This substitution caused an increase in the amount of V^{4+}, detected by XPS.

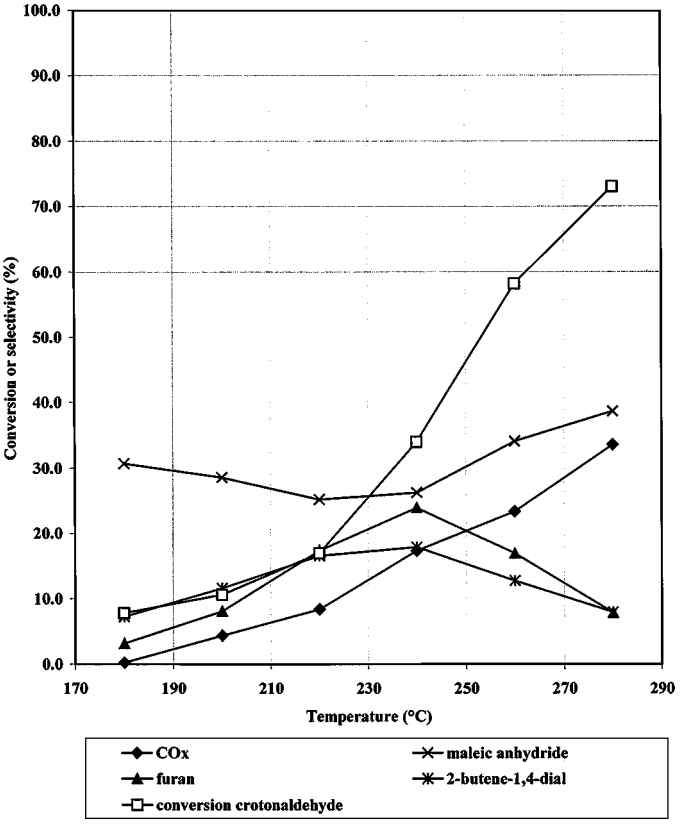

FIG. 10. Effect of temperature between 180 and 280°C for crotonaldehyde-selective oxidation over Catalyst B. Total gas flow rate was 105 sccm (0.15% crotonaldehyde in air and He).

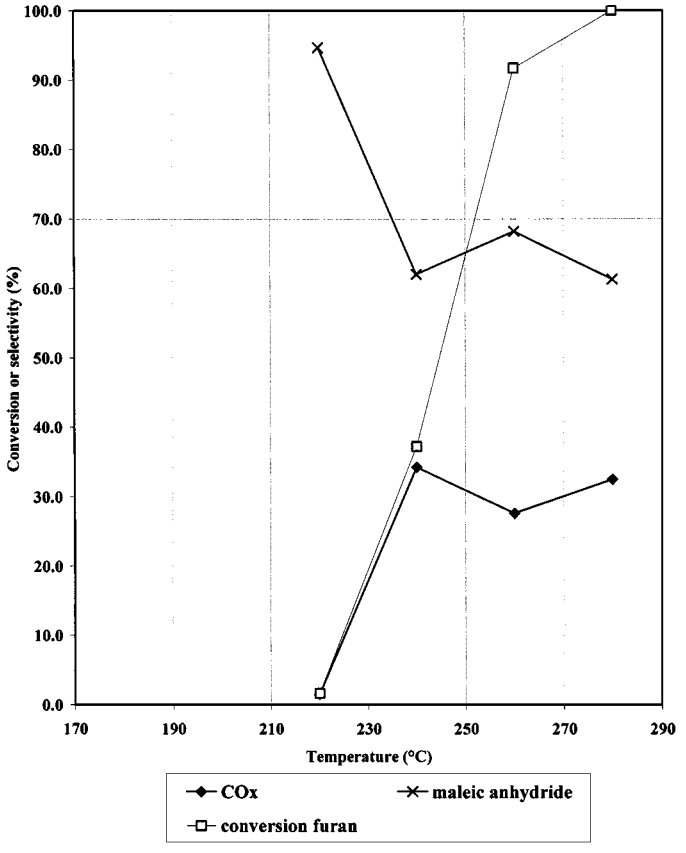

FIG. 11. Effect of temperature between 180 and 280°C for furan-selective oxidation over Catalyst B. Total gas flow rate was 105 sccm (0.15% furan in air and He).

Substitution of Mo into the V_2O_5 structure should involve reduction of V since Mo^{6+} replaces V^{5+}. Bielanski *et al.* used EPR studies to confirm the V^{5+} to V^{4+} transformation: further reduction to V^{3+} was also believed to occur (21). No evidence of V^{3+} was observed in XPS spectra of our catalysts.

For the VMoO catalysts, an increase in the availability of oxygen resulting from Mo incorporation into the V_2O_5 lattice has been attributed to reduction of V^{5+} to V^{4+} (22). The oxygen associated with these reduced vanadium cations was suggested to be more readily available for nucleophilic oxygen insertion. This postulate appeared to be true using VMoO catalysts as well. The reduction of V^{5+} to V^{4+} facilitated by Mo^{6+} incorporation allows additional V^{4+}–O sites to be available to form maleic anhydride. XPS analysis of the postreaction catalyst with lower molybdenum content (Catalyst A) showed a higher relative V^{4+} concentration than postreaction Catalyst B. This indicates that the surface of Catalyst A experienced significant reduction, while the surface of Catalyst B was only slightly reduced. A plausible explanation for this behavior is an increase in reoxidation capacity resulting from the presence of the Mo^{6+} species. If this is the case, the higher Mo content in catalyst B would replenish the catalyst with oxygen at a higher rate, therefore decreasing the extent of reduction during the selective oxidation process. This also may assist in the production of maleic anhydride from furan, as two additional oxygen atoms are necessary to complete this conversion.

Since electrophilic and nucleophilic oxidation transformations are required in this mechanism, the V_2O_5-based structure must have multiple active sites that are responsible for distinct steps in the reaction pathway. Three different coordinations of oxygen in the orthorhombic V_2O_5 structure have been considered to be reactive for catalytic oxidation: corner-sharing V–O–V, edge-sharing V–O, and terminal V=O. In Raman studies performed by Ono *et al.* for *n*-butane oxidation, edge-sharing V–O were enriched with ^{18}O by reoxidation of a reduced VMoO catalyst. Raman bands at 995, 701, and 521 cm^{-1} were assigned to terminal V=O, edge-sharing V–O, and corner-sharing V–O–V bonds, respectively, and ^{18}O incorporation into the catalyst caused a downward shift in the vibrational frequencies (23). Since the largest shift was observed for the 701 cm^{-1} peak, the V–O sites were believed to be responsible for oxygen

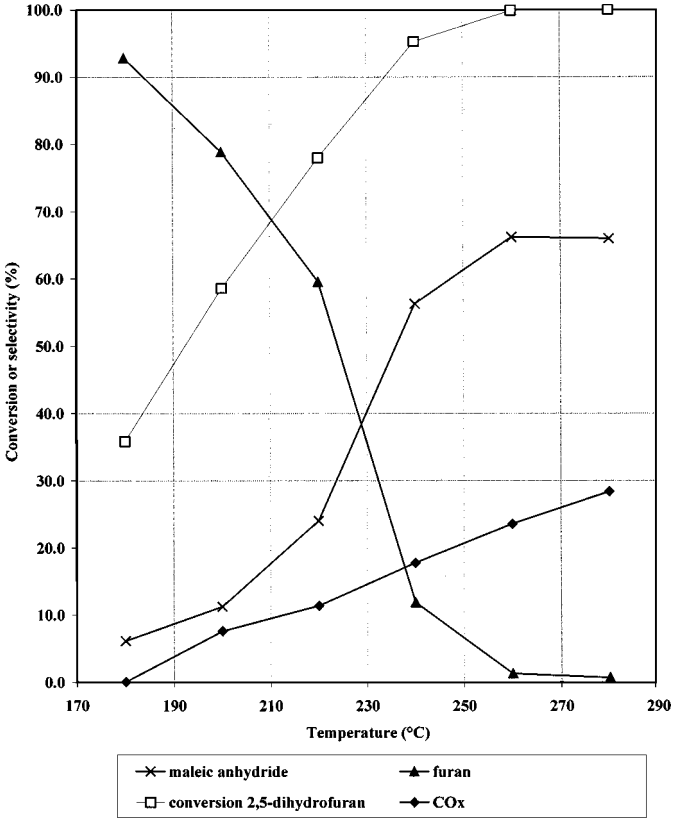

FIG. 12. Effect of temperature between 180 and 280°C for 2,5-dihydrofuran-selective oxidation over Catalyst B. Total gas flow rate was 105 sccm (0.15% 2,5-dihydrofuran in air and He).

insertion during *n*-butane oxidation. In contrast, IR studies have indicated that the V=O oxygen was the most reactive for benzene oxidation (24). For reducing conditions involving benzene, the IR band at 995 cm^{-1} (characteristic of the V=O oxygen) decreased in intensity and eventually disappeared over time. These disparate results, however, may not necessarily conflict with those of Ono: for a Mars–van Krevelen mechanism, the site responsible for oxygen insertion may not be the same site for oxygen reincorporation. In the V_2O_5 crystal structure, the vanadyl oxygen (V=O) species is considered to be the most electrophilic and could be responsible for the epoxidation of 1,3-butadiene. Surface oxygen (O^-, $2O^-$, etc.) species would likely also be active for electrophilic oxidation. However, lattice oxygen species (corner sharing V–O–V and edge sharing V–O) are more nucleophilic and are more likely to be involved in the formation of 2-butene-1,4-dial and maleic anhydride (25, 26).

The addition of water to the reactor 1,3-butadiene feed resulted in both higher conversion and selectivitiy to crotonaldehyde and furan. Several groups investigating the effect of water on C_3 hydrocarbon selective oxidation also observed selectivity changes due to water addition. These differences were mainly attributed to competitive adsorption between water and hydrocarbon intermediates (27, 28). Research performed by Ai *et al.* which focused on the oxidation of 1,3-butadiene to furan over supported heteropoly molybdates determined that the addition of water increased the reaction rate and the yield of furan (29). These researchers proposed that water (steam) removed strongly adsorbed products from the catalyst surface, which resulted in reactivation of catalytic sites and/or release of furan or other intermediates from the catalyst surface. In our studies, competitive adsorption of water may have occurred on specific VMoO catalyst sites where crotonaldehyde was bound as a reaction intermediate. This would explain the selectivity increase for crotonaldehyde when water is added. On the other hand, crotonaldehyde could simply have a lower energy for desorption and thus be the first to be released by the non-site-specific adsorption of water. Another explanation for the effect of water could be that the adsorption of water caused surface Brønsted acid sites to be formed which would promote isomerization. Further investigation of the effect of water will be reported in an additional publication.

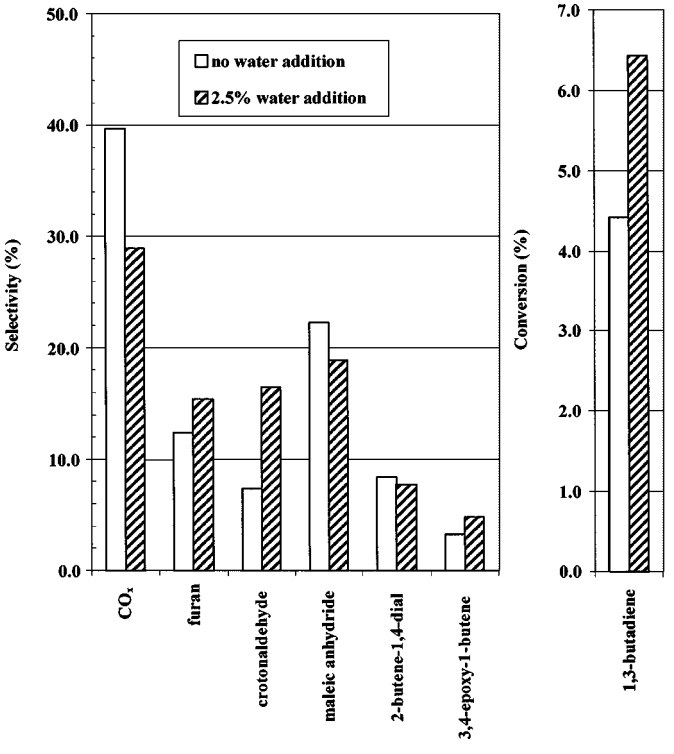

FIG. 13. Effect of water addition to reactant feed of 1,3-butadiene in air over Catalyst B. Total gas flow rate was 70 sccm (1.4% 1,3-butadiene in air and He).

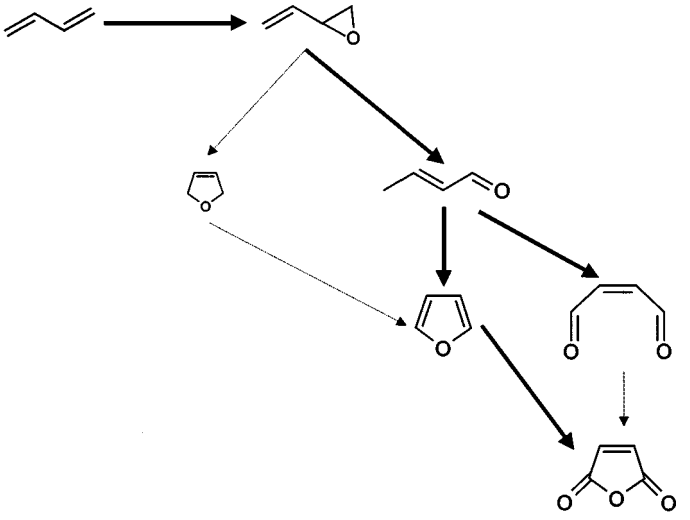

FIG. 14. Proposed reaction pathway for 1,3-butadiene to maleic anhydride over VMoO catalysts.

5. CONCLUSIONS

VMoO catalysts produced using a peroxide-based, sol–gel synthesis route resulted in the formation of solid solutions of Mo in V_2O_5 that could be characterized by several techniques such as XRD, LRS, and XPS. Of the materials evaluated for catalytic performance, the catalyst with the highest concentration of Mo was the most selective to maleic anhydride, while the catalyst with less Mo produced larger amounts of furan, crotonaldehyde, and CO_x. This effect was attributed to increased availability of nucleophilic oxygen associated with V^{4+}–O sites.

Based on experiments performed using 1,3-butadiene and several other product hydrocarbons as feeds, a reaction pathway was proposed for the selective oxidation of 1,3-butadiene to maleic anhydride, including an initial

1,2 addition of oxygen to 1,3-butadiene to produce 3,4-epoxy-1-butene and a dual pathway from crotonaldehyde to produce furan or 2-butene-1,4-dial.

ACKNOWLEDGMENTS

The authors acknowledge Jim Anderegg of the Ames Laboratory for performing XPS experiments and for assisting interpretation. This research was performed under funding from Ames Laboratory—USDOE Contract W-7405-Eng-82.

REFERENCES

1. Centi, G., and Trifiro, F., *J. Mol. Catal.* **35**, 255 (1986).
2. Monnier, J. R., *in* "3rd World Congress on Oxidation Catalysis" (R. K. Grasselli, St. T. Oyama, A. M. Gaffney, and J. E. Lyons, Eds.), p. 135. Elsevier Science, Amsterdam, 1997.
3. Monnier, J. R., and Muehlbauer, P. J., U.S. Patent 5,081,096 (1992).
4. Roberts, J. T., Capote, A. J., and Madix, R. J., *J. Am. Chem. Soc.* **113**, 9848 (1991).
5. Akimoto, M., and Echigoya, E., *Bull. Chem. Soc. Jpn.* **48**, 3518 (1975).
6. Crew, W. W., and Madix, R. J., *J. Am. Chem. Soc.* **115**, 729 (1993).
7. Xue, Z., and Schrader, G. L., *J. Catal.* **184**, 87 (1999).
8. Hönicke, D., *J. Catal.* **105**, 10 (1997).
9. Hönicke, D., *J. Catal.* **105**, 19 (1997).
10. Fontenot, C. J., Wiench, J. W., Pruski, M., and Schrader, G. L., *J. Phys. Chem. B* **104**, 11622 (2000).
11. Fontenot, C. J., Wiench, J. W., Pruski, M., and Schrader, G. L., *J. Phys. Chem. B*, submitted for publication 2001.
12. Alonso, B., and Livage, J., *J. Solid State Chem.* **148**, 16 (1999).
13. Bradzil, J. F., Toft, M. A., Bartek, J. P., Teller, R. G., and Cyngier, R. M., *Chem. Mater.* **10**, 4100 (1998).
14. Abello, L., Husson, E., Repelin, Y., and Lucazeau, G., *Spectrochim. Acta* **39A/7**, 641 (1983).
15. Mendialdua, J., Casanova, R., and Barbaux, Y., *J. Electron Spectrosc. Relat. Phenom.* **71**, 249 (1995).
16. Chen, Y., Xie, K., and Liu, Z. X., *Appl. Surf. Surf.* **133**, 221 (1998).
17. Demeter, M, Neumann, M., and Reichelt, W., *Surf. Sci.* **454–456**, 41 (2000).
18. Levasseur, A., Vinatier, P., and Gonbeau, D., *Bull. Mater. Sci.* **22**, 607 (1999).
19. Kihlborg, L., *Acta Chem. Scand.* **21**, 2495 (1967).
20. Hirata, T., and Zhu, H.-Y., *J. Phys.: Condens. Matter* **4**, 7377 (1992).
21. Bielanski, A., Dyrek, K., Kracik, I., and Wenda, E., *Bull. Pol. Acad. Chem.* **19**, 512 (1971).
22. Bielanski, A., and Najbar, M., *Appl. Catal. A* **157**, 223 (1997).
23. Ono, T., and Numata, H., *J. Mol. Catal. A* **116**, 421 (1997).
24. Bielanski, A., and Inglot, A., *React. Kinet. Catal. Lett.* **6/1**, 83 (1977).
25. Haber, J., Witko, M., and Tokarz, R., *Appl. Catal. A* **157**, 3 (1997).
26. Witko, J. M., Tokarz, R., and Haber, J., *Appl. Catal. A* **157**, 23 (1997).
27. Tichý, J, Küstka, J., and Machek, J., *Collect. Czech. Chem. Commun.* **48**, 698 (1983).
28. Stein, B., Weimer, C., and Gaube, J., *in* "3rd World Congress on Oxidation Catalysis," B.V. (R. K. Grasselli, St. T. Oyama, A. M. Gaffney, and J. E. Lyons, Eds.), p. 393. Elsevier Science, Amsterdam, 1997.
29. Ai, M., *J. Catal.* **67**, 110 (1981).